J Mater Sci (2010) 45:1385–1392
DOI 10.1007/s10853-009-4096-1

Improved structural stability of titanium-doped β-Bi_2O_3 during visible-light-activated photocatalytic processes

Yan Wang · Yanyuan Wen · Hanming Ding · Yongkui Shan

Received: 17 July 2009 / Accepted: 28 November 2009 / Published online: 10 December 2009

Abstract Due to its strong absorption to visible light and intrinsic polarizability, β-Bi_2O_3 could be a promising candidate for the visible-light-activated photocatalysis. However, its structural instability during a photocatalytic process prevents it from being used practically. In this work, titanium-doped β-Bi_2O_3 was synthesized by a hydrothermal method with subsequent calcination under 400 °C. Its crystal structure, photophysical property, and structural stability were investigated by using powder X-ray diffraction, Raman, infrared and diffuse reflectance UV–vis spectroscopies. The crystal structure of the titanium-doped β-Bi_2O_3 is analogous to β-Bi_2O_3. These two oxides exhibited comparable photocatalytic activities on the photodegradation of indigo carmine, rhodamine B, and methylene blue under visible-light irradiation. However, unlike β-Bi_2O_3, the titanium-doped β-Bi_2O_3 was quite stable during these photocatalytic reactions. The improvement in structural stability was attributable to the substitution of titanium species in the host crystal lattice. The current investigation results point toward the possibility of metal ion-doped bismuth oxides as efficient visible-light-activated photocatalysts.

Introduction

Semiconductor photocatalysts have attracted increasing attention during the past decade because of their potential applications in water cleavage, photodegradation of organic pollutants in air or water, disinfection/sterilization, and self-cleaning [1]. An efficient photocatalyst has to satisfy at least two prerequisites: (a) appropriate band structure for adequate utilization of solar energy, especially visible light that accounts for about 45% of the whole solar energy reaching the earth's surface; and (b) effective separation of photogenerated electron–hole pairs and subsequently fast diffusion of these charge carriers from the bulk to the reaction sites on the surface of the photocatalyst.

To develop photocatalysts that can operate effectively under visible-light irradiation, various approaches have been pursued to design and/or modify the band structures of the photocatalysts, such as metal ion implantation [2], cation and/or anion doping [3, 4], complex oxide formation [5, 6], surface plasmon resonance [7], and so on. Among these methods, the doping of TiO_2 with a variety of cations or anions has been extensively investigated, and the formation of complex metal oxides consisting of cations with d^0 or d^{10} electronic configuration has been well-studied [8]. Meanwhile, in order to promote the separation of photogenerated electron–hole pairs, several protocols have been tried, including the introduction of electron or hole scavengers [9], metal ion doping producing electron/hole trappers in the bulk [10], noble metal deposition acting as surface electron trapping [11], sensitization with a narrow band-gap semiconductors or dyes [12], and the exertion of an extra electric field [13]. In addition, the formation of wide and well-dispersed valence and conduction bands would also increase the mobility of both the photogenerated electrons and holes [14].

Bismuth (III) oxides with band gaps varying from 2.1 to 2.8 eV have optical absorption in the visible region [15–17]. Their intrinsic polarizabilities induced by Bi $6s^2$ lone electron pairs are favorable for the separation of photogenerated electron–hole pairs and the transfer of

Y. Wang · Y. Wen · H. Ding (✉) · Y. Shan
Department of Chemistry, East China Normal University, 3663 North Zhongshan Road, Shanghai 200062, People's Republic of China
e-mail: hmding@chem.ecnu.edu.cn

these charge carriers [18]. Furthermore, their wide delocalized bands are beneficial to the diffusion of photogenerated charge carriers [14, 17]. In view of these above advantages, Bi_2O_3 could be a promising candidate for the visible-light-activated photocatalysis. Bi_2O_3 can form six polymorphs, including two stable phases and four metastable ones [19–21]. These metastable phases are easily transformed to α phase at low temperatures and δ phase at high temperatures. Some of them have recently been employed in photocatalytic reactions [22–30], but they were proven unstable in these processes. Structural transformations from β to α phase, and further to bismuth carbonate, $(Bi_2O_2)CO_3$, were observed [27, 28]. These results suggested that Bi_2O_3 was not a suitable photocatalyst due to its chemical instability. As the introduction of traces of impurities can favor the stabilization of metastable phases of Bi_2O_3 at low temperature [20], ion doping could be an effective way to stabilize the crystal structures during the photocatalytic reactions.

In the current article, titanium (Ti)-doped β-Bi_2O_3 was prepared and employed as a photocatalyst. The relationship between its structure and photocatalytic activity, as well as its structural stability during the photocatalytic reactions were investigated and discussed.

Experimentals

Sample preparation

In a typical procedure, 8.75 g bismuth nitrate pentahydrate ($Bi(NO_3)_3{\cdot}5H_2O$, analytical grade) was dissolved in 15 mL acetic acid (50% v/v in water); then 2.0 mL tetrabutyl titanate ($Ti(OC_4H_9)_4$, chemical grade) was added dropwise to this solution under continuously stirring, forming a transparent solution. Subsequently, 15 mL isopropanol aqueous solution (20% v/v) was added into the above solution under magnetic stirring. The mixed solution was then transferred into a Teflon-lined stainless-steel autoclave up to 70% of its capacity. The sealed autoclave was heated to 140 °C and kept at such temperature for 1 h, then allowed to cool to room temperature. The resultant precipitation was filtered and washed with distilled water several times, and then dried in air at 70 °C for 1 h. The product was milled and calcined in air under a certain temperature with a constant heating rate of 10 °C/min and then held at this temperature for 2 h. The Ti-doped β-Bi_2O_3 (the ratio of Bi/Ti is about 20:1 in mole) was obtained when the calcination temperature was chosen as 400 °C, while bismuth titanium oxides, namely $Bi_4Ti_3O_{12}$ and $Bi_{12}TiO_{20}$, were formed at elevated calcination temperatures. $(Bi_2O_2)CO_3$ was prepared by slowly adding an acidic solution of $Bi(NO_3)_3{\cdot}5H_2O$ to excess Na_2CO_3 solution under vigorous stirring. $(Bi_2O_2)CO_3$ precipitate was filtered, washed, and dried in air. Pure β-Bi_2O_3 was prepared by heating $(Bi_2O_2)CO_3$ in air at 380 °C for 1.5 h. Degussa P25 TiO_2 (about 80% anatase/20% rutile) was purchased from Degussa (China) Co., Ltd. Pure α-Bi_2O_3 was purchased from Shanghai Chemicals Reagent Co., Ltd.

Characterization and measurements

The crystal structure was identified with a Rigaku D/Max-RB X-ray diffractometer with Ni-filtered Cu Kα radiation ($\lambda = 1.54056$ Å). Diffuse reflectance spectrum was recorded with a Shimadzu 2450 solid-state UV–vis spectrophotometer equipped with an integrating sphere diffuse reflectance accessory. Fourier transform infrared (IR) spectrum was recorded from KBr pellet in a Nicolet Nexus 670 spectrophotometer. Raman spectrum was acquired using an Acton SpectraPro 750i spectrographer.

The photodegradation of three dye molecules, namely indigo carmine, rhodamine B, and methylene blue, was used to evaluate the photocatalytic activities of the photocatalysts. Photocatalytic experiments were carried out in a homemade reactor, which was surrounded with a cooling system to keep the photocatalytic reaction system at room temperature. A 500 W halogen lamp with a KenKo L41 UV filter ($\lambda > 410$ nm) was used as a visible light source, and fixed 10 cm away from the reaction system. 0.1 g of photocatalyst was suspended in 100 mL of a dye solution with a concentration of 20 mg/L under magnetic stirring. The reaction system was first kept in the dark for 1 h to establish an adsorption–desorption equilibrium, and then exposed to the visible light. At the desired time intervals, 2 mL aliquots from each sample were taken, followed by centrifugation and filtration to remove the catalyst. The supernatant was used to determine the concentration of residual dye in solution. The decolorization of each dye was determined by measuring the change in its characteristic optical absorbance using a UV-1700 UV–vis spectrophotometer.

Results and discussion

Phase formation

The powder X-ray diffraction (XRD) patterns of various bismuth titanium oxides calcined at elevated temperatures are shown in Fig. 1. The pattern feature of Ti-doped β-Bi_2O_3 (calcined at 400 °C) is very close to those of pure β-Bi_2O_3 phase (JCPDS no. 27-0050) and some rare-earth metal ion-doped Bi_2O_3 oxides [21]. β-Bi_2O_3 is a metastable tetragonal phase that exists at moderate temperatures between 330 and 650 °C, and could be stabilized to room

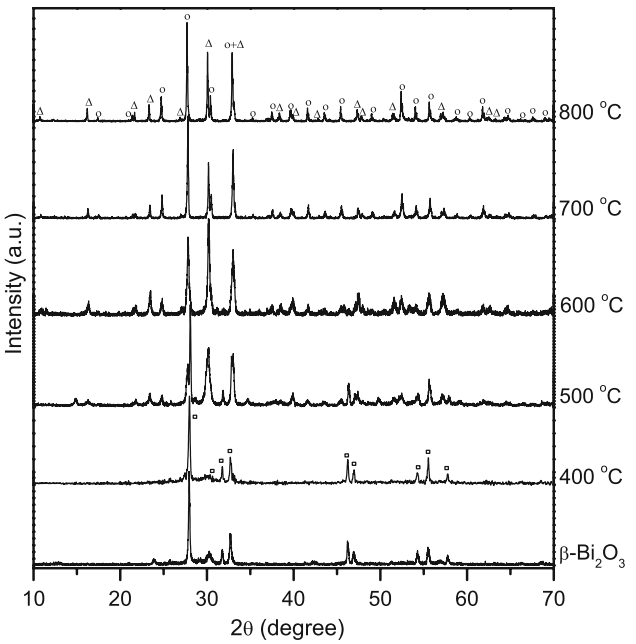

Fig. 1 XRD patterns of pure β-Bi_2O_3 and various bismuth titanium oxides calcined at elevated temperatures (°C). *Open square* Ti-doped β-Bi_2O_3, *open triangle* $Bi_4Ti_3O_{12}$, and *open circle* $Bi_{12}TiO_{20}$

temperature by partial substitution with other metal cations [20, 31, 32]. In this current work, titanium species were introduced to stabilize the β-Bi_2O_3 phase by way of the partial replacement of Bi atoms with Ti atoms. Since the ionic radius of bismuth ion (103 pm) is much larger than that of titanium ion (61 pm for coordination number of 6), the lattice will be compressed around the Ti impurity. Consequently, the host lattice will become dislocated and distorted remarkably. However, the degree of substitution should be very limited as the XRD pattern of the Ti-doped β-Bi_2O_3 is nearly identical to that of β-Bi_2O_3, and no TiO_2 crystal phase was detected.

β-Bi_2O_3 belongs to the space group of *P*-421c (114) and has a distorted defect structure with 25% of ordered vacant oxygen sites along (001) planes [33]. The Bi–O bond lengths varying from 0.2096 to 0.2463 nm were caused by this distorted structure. In β-Bi_2O_3, BiO_4(lp) trigonal bipyramids (lp = equatorial lone-pair electron) are connected via oxygen atoms at corners giving a network with empty channels [33]. The $6s^2$ lone-pair electrons of Bi^{3+} pointing towards these channels lead to a very high polarizability of the cation network. The good ionic conductivity of β-Bi_2O_3 with mobile oxide ions as the majority carriers should originate from such high polarizability [20]. The high polarizability should also be able to promote the separation and diffusion of photogenerated charge carriers. On the other hand, these heavily distorted polyhedra generally bring about thermodynamic instability of the crystal structure. However, β-Bi_2O_3 could be stabilized at low temperature by introducing traces of impurities [20, 31, 32]. Since the structural transition from β to α phase is associated with the rearrangement of Bi–O bonds [34], the lattice dislocation induced by Ti-substitution may impede this rearrangement and shorten Bi–Bi distances, thus stabilize the metastable phase down to room temperature.

The Ti-doped β-Bi_2O_3 was formed at 400 °C, and was converted to other phases at higher temperatures. The effect of calcination temperature on the structural change was demonstrated in Fig. 1. When the temperature was increased up to 500 °C, orthorhombic $Bi_4Ti_3O_{12}$ phase (JCPDS no. 35-0795) appeared. Between 550 and 800 °C, mixed phases of $Bi_4Ti_3O_{12}$ and cubic $Bi_{12}TiO_{20}$ (JCPDS no. 34-0097) were observed. Above 700 °C, $Bi_{12}TiO_{20}$ phase was predominant. These two phases could coexist even up to 900 °C [35]. High-temperature calcination resulted in a decrease in the mole of Bi_2O_3 because of the high volatility of bismuth and bismuth oxide constituents. The above results clearly manifested that the crystal structure of bismuth-based oxides is very sensitive to the calcination temperature. Although both $Bi_4Ti_3O_{12}$ and $Bi_{12}TiO_{20}$ have already been used as photocatalysts in several photocatalytic reactions [36, 37], their photocatalytic performances under visible-light irradiation were not satisfied.

As seen in Fig. 2, Raman spectrum of β-Bi_2O_3 is similar to that of niobia-stabilized β-Bi_2O_3 (Bi:Nb = 60:1) in ref. [31]. The bands centered at 229, 307, and 426 cm^{-1} are attributed to internal stretching modes of Bi–O bonds with the various bond lengths. However, the Raman spectrum of

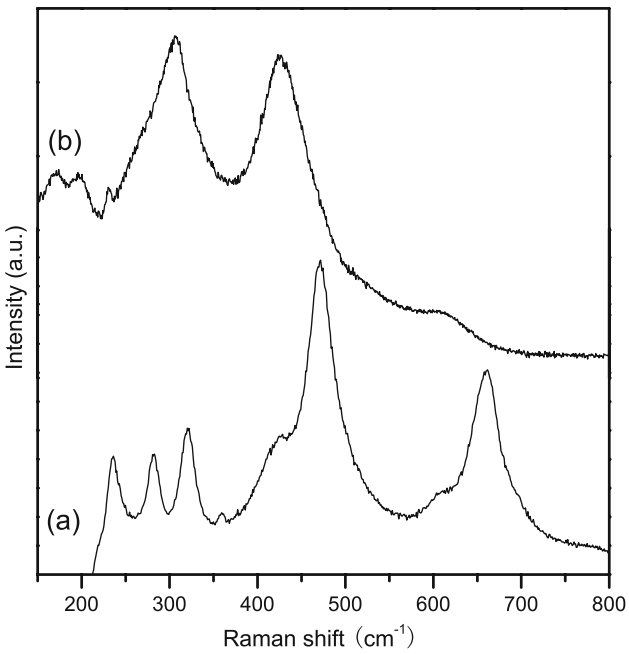

Fig. 2 Raman spectra of (*a*) Ti-doped β-Bi_2O_3 and (*b*) β-Bi_2O_3

the Ti-doped β-Bi_2O_3 is quite different, as shown in Fig. 2a. The peak at 426 cm^{-1} became weaker and two strong peaks around 472 and 661 cm^{-1} appeared. The changes in intensity and number of Raman peaks should be associated with the lowering of lattice symmetry induced by the doping of titanium ions. As Bi–O polyhedra were further distorted, the Bi–O bonds became shorter or longer in length. As a result, the Bi–O stretching modes shifted to higher or lower wavenumbers and the number of Raman peaks increased. The lack of Ti–O stretching modes further proved that the substitution was restricted.

Infrared spectroscopy was used to further clarify the structure of the Ti-doped β-Bi_2O_3. As shown in Fig. 3, two oxides exhibited similar IR spectroscopic characteristics except at the low frequencies. The band centered at 540 cm^{-1} is assigned to the Bi–O–Bi stretching vibration, and the one around 632 cm^{-1} can be attributed to the Bi–O stretching vibration of non-bridging oxygen of the distorted Bi–O polyhedra [38]. The bands appearing at high frequencies are associated with CO_2 and O_2 molecules adsorbed onto β-Bi_2O_3. The strongest band at 1,384 cm^{-1} is ascribable to the symmetric stretching vibration of CO_2 molecules, which is inactive in the IR spectrum of the free molecule, but becomes IR active due to the interaction between CO_2 molecules and β-Bi_2O_3. Other vibrational modes at 1,630 and 1,263 cm^{-1} are assigned to surface carbonate species [39]. The band at 1,102 cm^{-1} is attributed to O–O stretching mode when O_2 molecules are coordinated to β-Bi_2O_3 [40]. As there is plenty of vacant oxygen sites in β-Bi_2O_3 [20, 40], CO_2 molecules could be readily adsorbed on these coordinatively unsaturated sites and interact with β-Bi_2O_3, further forming carbonates on the surface. Due to the low partial pressure of CO_2 in air, the surface reaction should be very limited. However, an obvious change from β-Bi_2O_3 to $(Bi_2O_2)CO_3$ may happen if plenty of CO_2 molecules are available. It was revealed from the IR spectroscopic measurements that the Ti-doped β-Bi_2O_3 had also a strong affinity to CO_2 molecules.

Photophysical property

The UV–vis diffuse reflectance spectra of the Ti-doped β-Bi_2O_3 and β-Bi_2O_3 are displayed in Fig. 4. In both cases, an optical absorption up to 550 nm was observed. β-Bi_2O_3 was found to be an indirect band gap semiconductor at room temperature [15]. The optical absorbance of an indirect band gap semiconductor near the band edge follows an equation of $(\alpha h\nu)^{1/2} = A(h\nu - E_g)$, where α, h, ν, E_g, and A are the absorption coefficient, Planck constant, light frequency, band gap, and a constant, respectively [41]. The band gap of β-Bi_2O_3 was estimated to be 2.1 eV by plotting $(\alpha h\nu)^{1/2}$ versus $h\nu$, which is comparable to those previously reported values [16, 27, 42]. Besides the band-to-band transition, a tapering tail extending nearly to 750 nm was noted in both the cases. Its origin is currently not clear and may be associated with the presence of intrinsic lattice defects discussed above. Moreover, an additional absorption below 500 nm was observed in the case of the Ti-doped β-Bi_2O_3, which should originate from impurity levels as a result of the substitution of titanium ions.

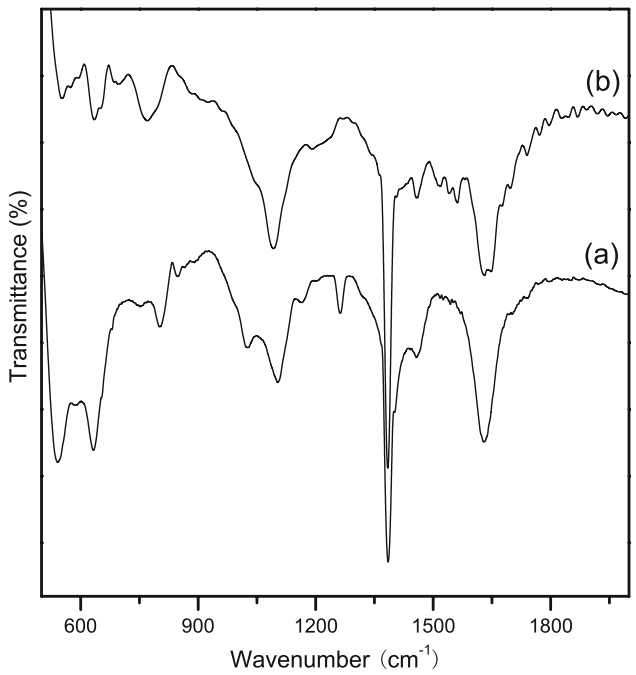

Fig. 3 Infrared spectra of (*a*) Ti-doped β-Bi_2O_3 and (*b*) β-Bi_2O_3

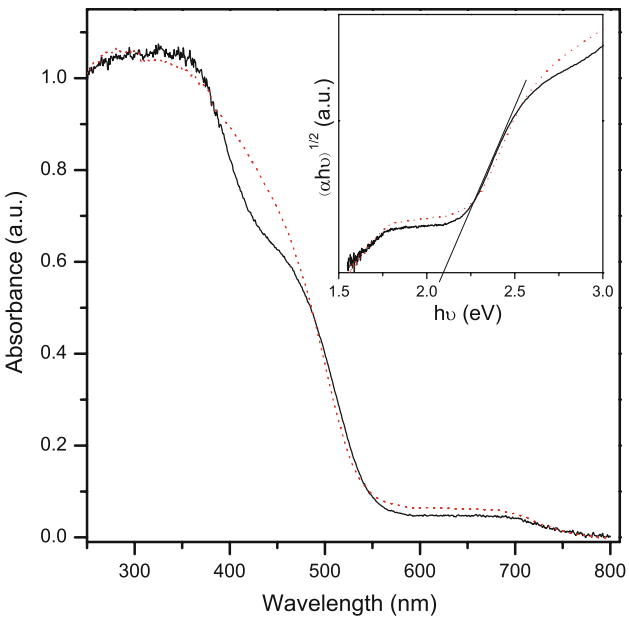

Fig. 4 UV–vis diffuse reflectance spectra of (*a*) Ti-doped β-Bi_2O_3 (*solid line*) and (*b*) β-Bi_2O_3 (*dotted line*)

In β-Bi_2O_3, the valence band is composed of Bi 6s and O 2p (the top) orbitals, and the conductance band is formed mainly by Bi 6p orbitals with some contribution from O 2p orbitals [43]. The hybridization of Bi 6s or 6p and O 2p orbitals gives rise to a wide and less localized valence band or conductance band. These wide and dispersed bands will increase the mobility of photoexcited charge carriers in both of the bands. In the Ti-doped β-Bi_2O_3, the empty Ti 3d orbitals are possible to contribute to the conductance band and make it wider. However, the energy level of Ti 3d is a little higher than that of Bi 6p orbital, and consequently, an empty state locating slightly above the lower level of the conductance band was formed. Thus, more energy is needed if a transition happens from the valence band to such state, which should be the origin of the blue-shifted absorption edge in the Ti-doped β-Bi_2O_3.

Photocatalytic performance

In order to evaluate photocatalytic property of the Ti-doped β-Bi_2O_3 under visible-light irradiation, indigo carmine, rhodamine B, and methylene blue in aqueous solutions were used as substrates. For comparison, pure α-Bi_2O_3, β-Bi_2O_3, and Degussa P25 (TiO_2) were chosen as the reference photocatalysts. Figure 5 shows the photodegradation results of the anionic dye of indigo carmine catalyzed by all the catalysts. In the absence of a photocatalyst, the indigo carmine molecules were slowly photobleached with about 4.7% fade in 1 h. Both the Ti-doped β-Bi_2O_3 and β-Bi_2O_3 exhibited strong adsorptive capacities to the indigo carmine molecules. As a result, the dye solution became pale and the photocatalyst turned light green when a photocatalytic system was kept in the dark for 60 min. Then the photocatalyst quickly recovered to its original yellow color under visible-light radiation, indicating that the photocatalytic process occurred over the surface of the photocatalyst. The dye solution became nearly colorless under further light irradiation. It can be seen that the Ti-doped β-Bi_2O_3 and β-Bi_2O_3 showed comparable photocatalytic activities, which were much better than α-Bi_2O_3 and Degussa P25. α-Bi_2O_3 displayed moderate adsorptive capacity and lower photodegradation rate than β-Bi_2O_3 owing to its stable and less-defect crystal structure.

Considering its strong absorbability, it is not appropriate that indigo carmine was used as the only substrate to judge the photocatalytic activity of the Ti-doped β-Bi_2O_3 objectively. As the Ti-doped β-Bi_2O_3 has poor adsorptive ability to cationic dye molecules, two cationic dyes of rhodamine B and methylene blue were chosen to further investigate the photocatalytic activities of the Ti-doped β-Bi_2O_3. The results are given in Figs. 6 and 7. In both cases, the photolytic fade without a catalyst under visible-light irradiation was less than 2% in 3 h. As seen from these figures, the photodegradation rate of rhodamine B was slower than indigo carmine, but little faster than methylene blue in the presence of all the photocatalysts. Indigo carmine was decolored faster than rhodamine B and methylene blue, which is due to its sensitization effect and strong affinity to

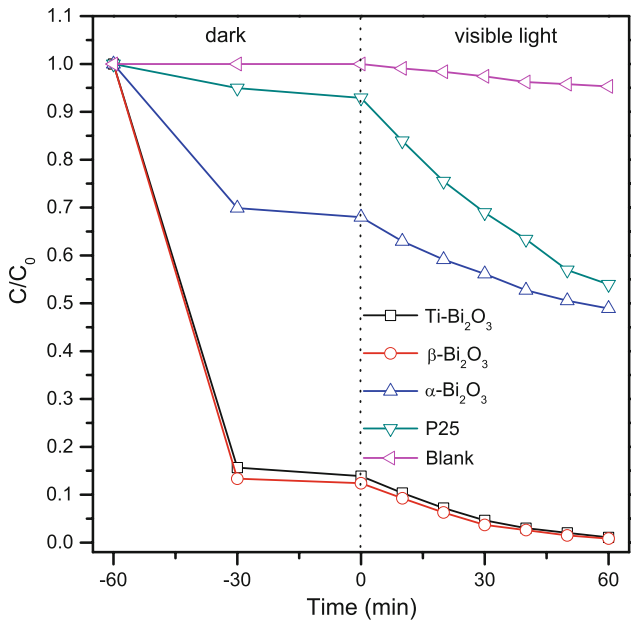

Fig. 5 Photodecomposition of indigo carmine in solution in the presence of various photocatalysts and without a photocatalyst under visible-light irradiation. C is the concentration of the dye at time t, and C_0 is the initial concentration of the dye (the same in Figs. 6, 7)

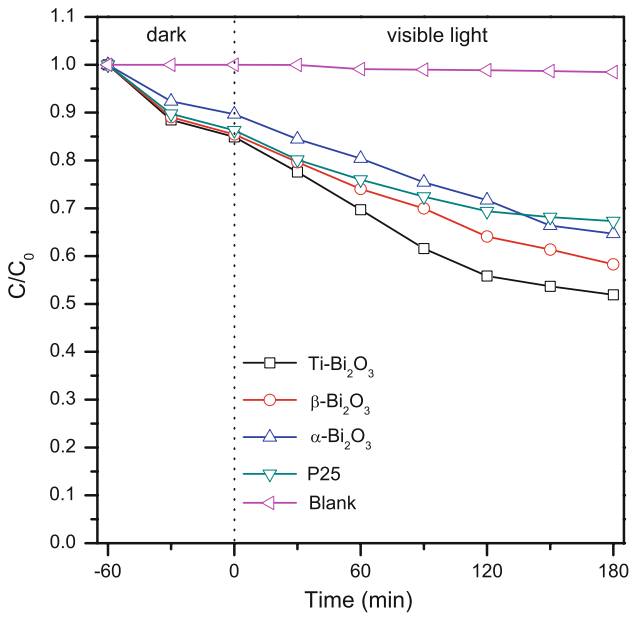

Fig. 6 Photodecomposition of rhodamine B in solution in the presence of various photocatalysts and without a photocatalyst under visible-light irradiation

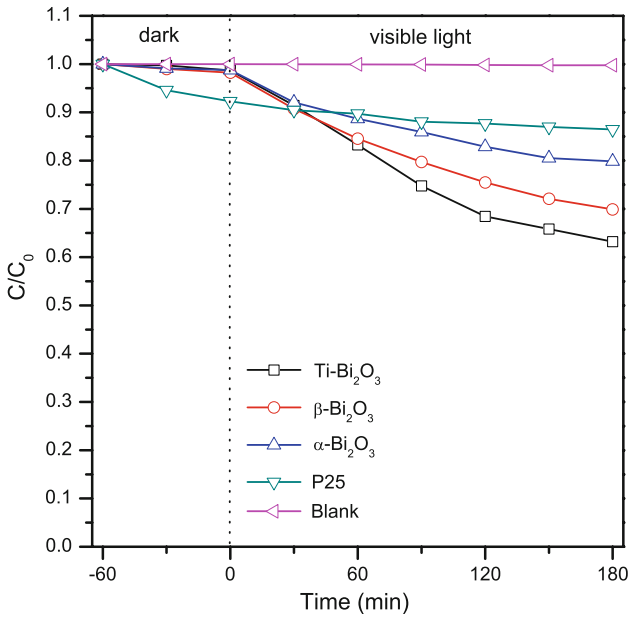

Fig. 7 Photodecomposition of methylene blue in solution in the presence of various photocatalysts and without a photocatalyst under visible-light irradiation

the photocatalysts. Generally, anionic dye of indigo carmine is readily adsorbed by oxides due to the plenty of positively charged defects on their surfaces, while cationic dyes of rhodamine B and methylene blue are not easily adsorbed. This fact implied that the previous adsorption process was very important during a photocatalytic reaction. In addition, the Ti-doped β-Bi_2O_3 showed a little faster photocatalytic reaction rate than β-Bi_2O_3 in both photocatalytic reactions, indicating that Ti-doping could enhance the photocatalytic activity. This enhancement may be associated with the extra structural distortion and additional optical absorption.

It should be mentioned that Degussa P25 showed certain adsorptive capacities to all the dye molecules in the dark owing to its large specific surface area ($\sim$50 m^2/g). Although Degussa P25 cannot absorb visible light, it displayed degradation ability somewhat to indigo carmine and rhodamine B under visible-light irradiation due to the sensitization effect [44]. The presence of carboxylic or carboxylate groups in both dyes can enhance the adsorption on the surface of Degussa P25 and induce the sensitization effect. However, the lack of anchoring group in methylene blue made it hard to be degraded.

Structural stability

While it seems that, the Ti-doping had no apparent improvement on the photocatalytic activity of β-Bi_2O_3, it is important to clear that the substitution enhanced greatly the structural stability of β-Bi_2O_3 during the photocatalytic processes. Both α-Bi_2O_3 and β-Bi_2O_3 were reported previously not stable during the photocatalytic reactions, in which they gradually transformed to $(Bi_2O_2)CO_3$ or other new phases [27]. In order to investigate the structural stability of the Ti-doped β-Bi_2O_3, a definite amount of the photocatalyst was recycled in repeated photocatalytic experiments of indigo carmine decomposition and its structural change was monitored. As displayed in Fig. 8a, pure β-Bi_2O_3 is not stable in the repeated photocatalytic reactions. Even after one run, most of β-Bi_2O_3 was transformed to its α counterpart (JCPDS no. 65-2366), accompanied with the formation of $(Bi_2O_2)CO_3$ phase (JCPDS no. 41-1488). According to quantitative phase analysis based on the Reference Intensity Ratio (RIR) method [45], the weight percent of α-Bi_2O_3 is about 81%, $(Bi_2O_2)CO_3$ is 11%, while β-Bi_2O_3 is only 8%. The structural transition from β- to α-Bi_2O_3 could easily happen thanks to the fact

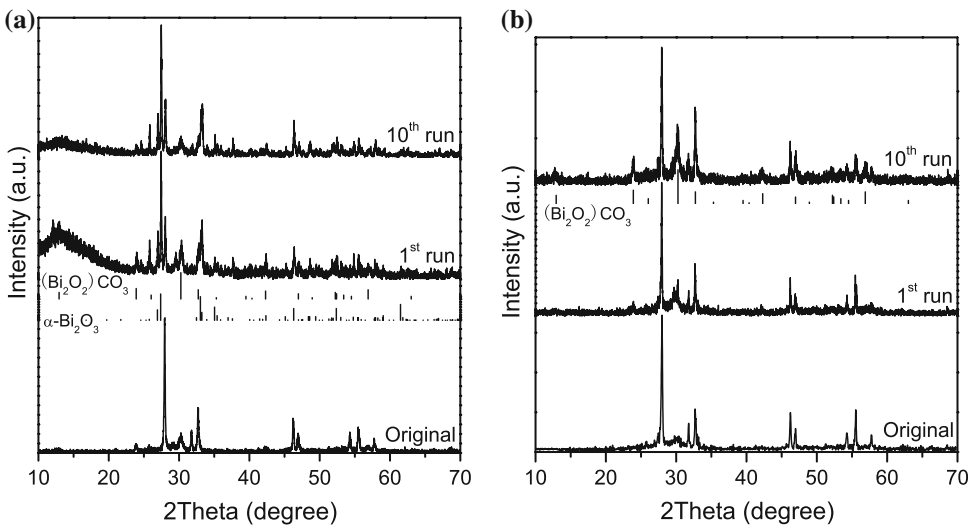

Fig. 8 Structural evolution of the photocatalyst during the repeated photocatalytic processes of the complete decomposition of indigo carmine with a concentration of 10 mg/L under visible-light irradiation: **a** β-Bi_2O_3 and **b** Ti-doped β-Bi_2O_3

that α-Bi_2O_3 was more stable at room temperature [20, 21]. Furthermore, a large amount of CO_2 molecules generated from the photodecomposition of the dye molecules would promote the formation of $(Bi_2O_2)CO_3$. A blank experiment leaving β-Bi_2O_3 in water under ambient atmosphere exhibited that negligible $(Bi_2O_2)CO_3$ was formed, indicating that the CO_2 molecules contributed to $(Bi_2O_2)CO_3$ was mainly derived from the photodegradation of indigo carmine, rather than the dissolution of the CO_2 gas in the air. In fact, the concentration of the dissolved CO_2 in water under ambient atmosphere is very low, about 1.02×10^{-5} mol/L.

As expected, the introduction of titanium species stabilized the crystal structure of β-Bi_2O_3 during the repeated photocatalytic reactions. The XRD patterns showing the structural change of the Ti-doped β-Bi_2O_3 reused for ten runs are presented in Fig. 8b. A trivial structural transformation from the Ti-doped β-Bi_2O_3 to $(Bi_2O_2)CO_3$ was observed, and no α phase was found in the first run. Based upon the RIR method, the weight percent of β-Bi_2O_3 is about 81%, and $(Bi_2O_2)CO_3$ is 19%. Considering the carbon balance in solution, the CO_2 molecules contributed to $(Bi_2O_2)CO_3$ was derived from the photodegradation of indigo carmine, suggesting that indigo carmine molecules were completely mineralized. After ten runs, the Ti-doped β-Bi_2O_3 is still the predominant phase, but the weight percent of $(Bi_2O_2)CO_3$ was increased to 35%. These results indicated that the structural transformation from β- to α-Bi_2O_3 was blocked and the formation of $(Bi_2O_2)CO_3$ was retarded. However, the photocatalytic activity of the Ti-doped β-Bi_2O_3 decreased slightly accompanied with the formation of more $(Bi_2O_2)CO_3$. A control experiment using $(Bi_2O_2)CO_3$ as a photocatalyst revealed that $(Bi_2O_2)CO_3$ had strong adsorptive capacity to the indigo carmine molecules, but had no photocatalytic activity under visible-light irradiation. Thus, the reduced photocatalytic activity was associated with the formation of $(Bi_2O_2)CO_3$.

$(Bi_2O_2)CO_3$ has a layered structure in which the carbonate layers are sandwiched between the $(Bi_2O_2)^{2+}$ layers [46]. During the thermal decomposition, CO_2 molecules are eliminated from the carbonate ions and O^{2-} ions are left in the interlayer of $(Bi_2O_2)^{2+}$ due to the polarization effect of $(Bi_2O_2)^{2+}$ to the polarizable carbonate anions, subsequently β-Bi_2O_3 is formed. This reaction generally takes place around 400 °C. The freshly prepared β-Bi_2O_3 shows a strong adsorptive ability to CO_2 molecules and a reverse reaction may happen. However, the reversible reaction was rarely reported in the literature although it has large tendency to occur in view of Gibbs energy change [47]. The transformation of α-Bi_2O_3 to $(Bi_2O_2)CO_3$ was described to occur by the addition of an alkali carbonate solution or excess CO_2 in a closed autoclave [47]. The structure of β-Bi_2O_3 is characterized by the presence of vacant oxygen sites, which offers the possibility to interact with CO_2 [40], so that the transformation from β-Bi_2O_3 to $(Bi_2O_2)CO_3$ may happen in similar experimental conditions. During the photocatalytic process, large amounts of CO_2 molecules generated from the decomposition of dye molecules could be adsorbed onto the surface of the Ti-doped β-Bi_2O_3 and further formed carbonates. In this way, the crystal phase of $(Bi_2O_2)CO_3$ was formed. Although due to the existence of empty channels in the lattice serving as diffusion paths, CO_2 molecules may diffuse into the interior of the Ti-doped β-Bi_2O_3 and interact with oxygen ions forming carbonate species on the inside, the bulk structural change is negligible considering the difficult diffusion of CO_2. This structural transformation should be confined mainly on the partial surface. This is the reason why only limited Ti-doped β-Bi_2O_3 was converted to $(Bi_2O_2)CO_3$ even after ten runs.

Conclusions

The Ti-doped β-Bi_2O_3 was prepared and used as a photocatalyst in the present work. The photocatalyst exhibited reasonable photocatalytic activities on the photodegradation of three dye molecules under visible-light irradiation. Such activities are associated with its optical absorption up to 550 nm with a tail extending to 750 nm, the intrinsic polarizability induced by the distorted Bi–O polyhedra, and the introduction of titanium species inside the host lattice. More importantly, compared to β-Bi_2O_3, the Ti-doped β-Bi_2O_3 was more stable during the photocatalytic processes, because the introduction of titanium species stabilized its host crystal lattice greatly. This fact provides us some inspirations to pursue highly efficient visible-light-activated photocatalysts. Just like the role of TiO_2 in UV-light-driven photocatalysis, Bi_2O_3 could be an excellent visible-light-activated photocatalyst due to its specific crystal structure and unique electronic configuration of Bi atoms. Considering that the distorted lattice usually results in the structural instability at lower temperatures or in photocatalytic reactions, appropriate doping with rare-earth elements or transition metals is an effective way to stabilize these distorted phases. In this sense, numerous doped Bi_2O_3 systems could be good candidates to be exploited as visible-light-activated photocatalysts.

Acknowledgements The work was supported by the key project of Shanghai Science and Technology Committee (No. 06DZ05025 and 08JC1408600), P. R. China. The anonymous reviewer was appreciated for his/her helpful suggestions.

References

1. Fujishima A, Honda K (1972) Nature 238:37
2. Yamashita H, Anpo M (2004) Catal Surv Asia 8:35

3. Hoffmann MR, Martin ST, Choi W, Bahnemann DW (1995) Chem Rev 95:69
4. Chen X, Mao SS (2007) Chem Rev 107:2891
5. Luan J-F, Hao X-P, Zheng S-R, Luan G-Y, Wu X-S (2006) J Mater Sci 41:8001. doi:10.1007/s10853-006-0869-y
6. Wang D, Kako T, Ye J (2008) J Am Chem Soc 130:2724
7. Wang P, Huang B, Qin X, Zhang X, Dai Y, Wei J, Whangbo MH (2008) Angew Chem Int Ed 47:1
8. Inoue Y (2006) In: Fierro JLG (ed) Metal oxides chemistry and applications. Taylor & Francis, Boca Raton, FL
9. Kim HG, Hwang DW, Lee JS (2004) J Am Chem Soc 126:8912
10. Linsebigler AL, Lu G, Yates JT (1995) Chem Rev 95:735
11. Shan Z, Wu J, Xu F, Huang FQ, Ding HM (2008) J Phys Chem C 112:15423
12. Peter LM, Wijayantha KGU, Riley DJ, Waggett JP (2003) J Phys Chem B 107:8378
13. Vinodgopal K, Kamat PV (1995) Sol Energy Mater Sol Cells 38:401
14. Tang J, Zou Z, Ye J (2007) J Phys Chem C 111:12779
15. Dolocan FI V (1981) Phys Status Solidi A 64:755
16. Leontie L, Caraman M, Delibas M, Rusu GI (2001) Mater Res Bull 36:1629
17. Walsh A, Watson GW, Payne DJ, Edgell RG, Guo J, Glans P-A, Learmonth T, Smith KE (2006) Phys Rev B: Condens Matter Mater Phys 73:235104
18. Lin X, Huang F, Wang W, Shi J (2007) Scr Mater 56:189
19. Medernach JW, Snyder RL (1978) J Am Ceram Soc 61:494
20. Shuk P, Wiemhöfer H-D, Guth U, Göpel W, Greenblatt M (1996) Solid State Ionics 89:179
21. Drache M, Roussel P, Wignacourt J-P (2007) Chem Rev 107:80
22. Gurunathan K (2004) Int J Hydrogen Energy 29:933
23. Bessekhouad Y, Robert D, Weber JV (2005) Catal Today 101:315
24. Zhang L, Wang W, Yang J, Chen Z, Zhang W, Zhou L, Liu S (2006) Appl Catal A 308:105
25. Hameed A, Montini T, Gombac V, Fornasiero P (2008) J Am Chem Soc 130:9658
26. Xie J, Xiaomeng L, Chen M, Zhao G, Song Y, Lu S (2008) Dyes Pigm 77:43
27. Eberl J (2008) Visible light photo-oxidations in the presence of bismuth oxides. Ph.D. Thesis, Friedrich-Alexander-Universität Erlangen-Nürnberg, Erlangen, Germany
28. Eberl J, Kisch H (2008) Photochem Photobiol Sci 7:1400
29. Zhou L, Wang W, Xu H, Sun S, Shang M (2009) Chem Eur J 15:1776
30. Chai SY, Kim YJ, Jung MH, Chakraborty AK, Jung D, Lee WI (2009) J Catal 262:144
31. Hardcastle FD, Wachs IE (1992) J Solid State Chem 97:319
32. Kharton VV, Naumovich EN, Yaremchenko AA, Marques FMB (2001) J Solid State Electrochem 5:160
33. Blower SK, Greaves C (1988) Acta Crystallogr C 44:587
34. Depero LE, Sangaletti L (1996) J Solid State Chem 122:439
35. Wada N, Morinaga K (1998) J Ceram Soc Jpn 106:576
36. Yao WF, Xu XH, Wang H, Zhou JT, Yang XN, Zhang Y, Shang SX, Huang BB (2004) Appl Catal B 52:109
37. Zhou J, Zou Z, Ray AK, Zhao XS (2007) Ind Eng Chem Res 46:745
38. Hazra S, Ghosh A (1995) Phys Rev B 51:851
39. Davydov AA (2003) Molecular spectroscopy of oxide catalyst surfaces. Wiley, Chichester, England
40. Barreca D, Morazzoni F, Rizzi GA, Scotti R, Tondello E (2001) Phys Chem Chem Phys 3:1743
41. Butler MA (1977) J Appl Phys 48:1914
42. Dolocan V (1978) Appl Phys A 16:405
43. Evarestov RA, Shapovalov VO, Veryazov VA (1994) Phys Status Solidi B 183:K15
44. O'Regan B, Gratzel M (1991) Nature 353:737
45. Hubbard CR, Snyder RL (1988) Powder Diffr 3:74
46. Greaves C, Blower SK (1988) Mater Res Bull 23:1001
47. Taylor P, Sunder S, Lopata VJ (1984) Can J Chem 62:2863